International Journal of Aviation Science and Engineering
e-ISSN: 2715-6958 p-ISSN: 2721-5342
AVIA

Original Article

Numerical Simulation of Droplet Behavior under Varying Density Ratios Using Finite Volume-Front Tracking Method

Dondi Kurniawan [1*], Yulia Venti Yoanita [2], Sinung Tirtha Pinindriya [3], Eli Kumolosari [4], Angga Darma Prabowo [1], M. Rangga Saputra [1]

[1] Department of Mechanical Engineering, Faculty of Engineering, University of Lampung, Gedung H Lt. 2, Jl. Prof. Soemnantri Brojonegoro No. 1, Bandar Lampung 35143, Indonesia
[2] Department of Automotive Technology Vocational Education, PGRI University of Yogyakarta, Jl. PGRI I Sonosewu No. 117, Yogyakarta 55182, Indonesia
[3] Research Center for Aeronautics Technology, National Research and Innovation Agency, Jl. Raya LAPAN, Sukamulya, Rumpin, Bogor, West Java 16350 Indonesia
[4] Department of Mechanical Engineering, Adisutjipto Institute of Aerospace Technology, Jl. Janti Blok - R Lanud Adisutjipto, Yogyakarta 55198, Indonesia
* Correspondence: dondikur17@eng.unila.ac.id

Received: 4 July 2024; Accepted: 1 November 2024; Published: 10 December 2024

The study of droplet dynamics is very important to understand the mechanism of heat, mass, and momentum transfer in two phases. One approach to studying this phenomenon is through numerical simulation. The front tracking method is one of the techniques often used in numerical simulation of droplets to handle phase interactions in multiphase flows. The characteristics of droplets when they collide with surfaces with different density values are the subject of this study. The modeling used in this study is an interface diffusion approach using 2 types of fluids that have different properties. The domain used is Square Box-Staggered Grid. The software used is MATLAB R2024a. The results of the study indicate that the value of density ratio has a significant effect on the spreading factor, apex height, spreading velocity and pressure.

Keywords: droplet, front tracking, multiphase flow, numerical study, density ratio

---

1. Introduction

Droplet is a two-phase phenomenon that is widely found in various applications in science and industry such as microfluidics, spray cooling, Fuel Combustion, and meteorology. The study of droplet dynamics is very important to understand the mechanism of heat, mass, and momentum transfer in two phases. One approach to studying this phenomenon is through numerical simulation, which allows in-depth analysis of the parameters that affect droplet behavior without the limitations of laboratory experiments [1]. In addition, other methods such as Direct Numerical Simulation (DNS) are also often used to understand droplet dynamics under various conditions, including evaporation and condensation [2].

Recent studies have addressed the effects of surface heterogeneity on droplet dynamics using numerical modeling. This study showed that super hydrophobic surfaces with certain heterogeneity cause droplets to experience anisotropic spreading and directional reflection [3]. This study shows that numerical modeling can help understand how surface properties affect droplet characteristics. Numerical simulations were also used to study the droplet velocity in constricted microchannel. Factors such as relative viscosity, capillary number and channel constriction ratio significantly affect the droplet velocity and control in these systems [4]. This understanding is essential in building of microfluidic instruments for biomedical and analytical chemistry applications.

Other studies conducted to explore the understanding of droplet dynamics focused on the interaction of droplets with magnetic fields using Boundary Element Method (BEM) simulations [5] and interactions between molecules in droplet systems based on molecular dynamics (MD) [6] . Both approaches have succeeded in providing a deep understanding of the characteristics of droplet dynamics and phenomena that occur in their applications.

Finite Volume Method (FVM) and Front Tracking are two techniques that are often used in numerical simulation of droplets to handle phase interactions in multiphase flows [7]–[9]. The Finite Volume Method allows solving conservation equations with a high degree of accuracy on a discrete grid, while the Front Tracking method is used to track the droplet interface explicitly against droplet deformation during spreading, breaking, or coalescence processes [9]. The combination of these two methods has been applied in studies of droplet impact on surfaces with varying degrees of wettability and heterogeneity [10]–[12], providing a deeper understanding of the physical mechanisms that occur at the microscopic scale.

This study is a development of what has been done by the author by investigating the characteristics of the density field [12], [13]. The results of this study have been validated with the research of Tryggvason 2012 [9]and compared with the results of the research of Wu et al. 2015 [14]and Endang et al. 2020 [11]. This goal of the study is to examine the characteristics of droplets when hitting surfaces with varying density values. The results of this study showed that the ratio of density had a significant consequences for the spreading factor, apex height, spreading speed and pressure.

2. Materials and Methods

2.1. Mathematical Modeling and Governing Equations

The modeling used in this study, the interface diffusion approach uses 2 types of fluids that have opposing properties. The simplification of the case can be described as a free-falling droplet hitting a surface that is in another fluid. This study is a development that researchers have done in 2018 and 2024. Overall, the present study is intended to determine the implications of surface tension involvement and variations in density ratio on spreading factor, apex height, spreading velocity and pressure. The fundamental formulas used are the continuity equation and Navier-Stokes for incompressible and unsteady cases. Droplet impacting the surface is modeled with the condition (d_d,v_o , θ) = (0.2 mm, 0.66 m/s, 90 °). The function of time is expressed by the dimensionless number $t^* = (tv_o/d_d)$.

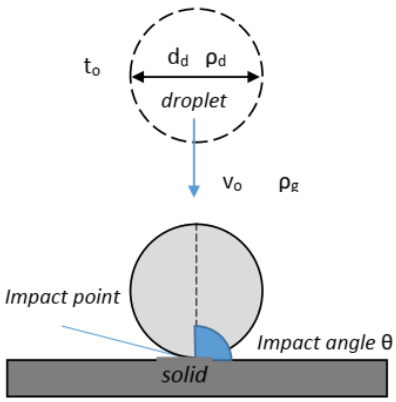

Figure 1. Scheme of droplets hitting a surface [12]

2.1.1. Computational Domain and Boundary Conditions

This study uses a box domain with length and width L_x and L_y, where the velocity is the boundary and the pressure is in the center of the domain in the control volume approach. Figure 2. a) shows the Staggered-Grid computational domain where the horizontal velocity is located at the left and right boundaries while the vertical velocity is at the upper and lower boundaries of the control volume [9].

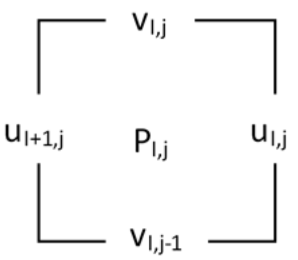

a)

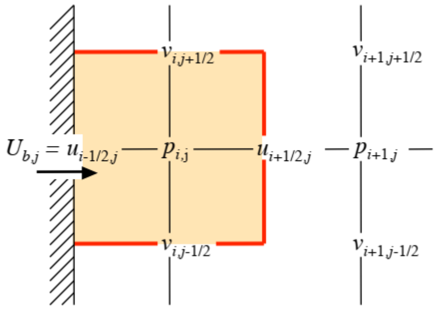

b)

Figure 2. a) Computational domain in staggered-grid notation b) Boundary conditions

To start the solution step, first determine the appropriate boundary conditions to facilitate the solution. Since the boundary and the center of the control volume are coinciding, we can adjust the velocity to the appropriate value. From figure 2. b) it is known that the Interpolation between the wall velocity and the known ghost velocity will give a value for the velocity in the domain. The equation on the boundary wall follows the following equation.

$$u_{wall} = (1/2)\left(u_{i,1} + u_{i,2}\right) \tag{1}$$

$$u_{i,1} = (1/2)\left(u_{wall} - u_{i,2}\right) \tag{2}$$

Where $u_{i,1}$ is the phantom velocity and u_{wall} is the tangential velocity at the wall. As long as the wall velocity and the velocity inside the domain, $u_{i,2}$, are known, we can quickly determine the ghost *velocity*.

2.1.2. Governing Equations

The governing equations used in this study are the continuity and Navier-Stokes equations. The equations used for the case of incompressible flow do not change and two-dimensional unsteady flow, so the governing equations are presented as follows,

$$\frac{\partial \rho}{\partial t} + \rho\left(\frac{\partial u}{\partial x} + \frac{\partial v}{\partial y}\right) = 0 \tag{3}$$

$$\frac{\partial u}{\partial t} + \mathrm{u}\frac{\partial u}{\partial x} + \mathrm{v}\frac{\partial u}{\partial y} = -\frac{1}{\rho}\frac{\partial p}{\partial x} + \nu\left(\frac{\partial^2 u}{\partial x^2} + \frac{\partial^2 u}{\partial y^2}\right) + g_x + f \tag{4}$$

$$\frac{\partial v}{\partial t} + \mathrm{u}\frac{\partial v}{\partial x} + \mathrm{v}\frac{\partial v}{\partial y} = -\frac{1}{\rho}\frac{\partial p}{\partial x} + \nu\left(\frac{\partial^2 v}{\partial x^2} + \frac{\partial^2 v}{\partial y^2}\right) + g_y + f \tag{5}$$

Where, the velocity in the x and y directions are represented by notation of u and v, p represents the value of pressure, $\rho$is the density and $\nu$is the viscosity value.

2.2. Numerical Algorithms and Discretization of Governing Equations

The governing equations are solved initially by neglecting the pressure value to simplify the problem. The governing equations are discretized using the *fractional-step method* which is done implicitly for each component of the x- and y-axis directions. The equations of the x- and y-axis directions are written in the following equations,

$$\frac{\partial u}{\partial t}=-\frac{\partial}{\partial x}\left(u^2\right)+\nu\frac{\partial^2 u}{\partial x^2}-\frac{\partial(uv)}{\partial y}+\nu\frac{\partial^2 u}{\partial^2 y}-\frac{\partial p}{\partial x}+g_x \tag{6}$$

$$\frac{\partial v}{\partial t}=-\frac{\partial}{\partial x}(uv)+\nu\frac{\partial^2 v}{\partial x^2}-\frac{\partial\left(v^2\right)}{\partial y}+\nu\frac{\partial^2 v}{\partial^2 y}-\frac{\partial p}{\partial y}+gy \tag{7}$$

2.2.1. Discretization of velocities in the x and y directions

Discretization of the x and y axis velocities is carried out in 2 stages using the fractional-step method of the Thomas algorithm.

First order fractional-step formulation as follow [15],

$$\frac{\hat{u}-u^n}{\Delta t}=-\frac{1}{\Delta x}\left([\hat{u}]^2{}_{i+1/2,j}-[\hat{u}]^2{}_{i-1/2,j}\right)+\nu.\frac{1}{\Delta x^2}\left(\hat{u}_{i+1,j}-2\hat{u}_{i,j}-\hat{u}_{i-1,j}\right) \tag{8}$$

$$\frac{\hat{v}-v^n}{\Delta t}=-\frac{1}{\Delta x}\left([\hat{u}\hat{v}]_{i+1/2,j}-[\hat{u}\hat{v}]_{i-1/2,j}\right)+\nu.\frac{1}{\Delta x^2}\left(\hat{v}_{i+1,j}-\hat{v}_{i,j}-\hat{v}_{i-1,j}\right) \tag{9}$$

Second order fractional-step formulation as follow [16], [17],

$$\frac{u^*-\hat{u}}{\Delta t}=-\frac{1}{\Delta y}\left([uv]^*{}_{i,j+1/2}-[uv]^*{}_{i,j-1/2}\right)+\nu\frac{1}{\Delta y^2}\left(u^*{}_{i,j+1}-2u^*{}_{i,j}-u^*{}_{i,j-1}\right)$$
$$-\frac{1}{\Delta x}\left(p^n{}_{i+1/2,j}-p^n{}_{i-1/2,j}\right)+f_y^{n+1/2} \tag{12}$$

$$\frac{v^*-\hat{v}}{\Delta t}=-\frac{1}{\Delta y}\left(\left[v^2\right]^*{}_{i,j+1/2}-\left[v^2\right]^*{}_{i,j-1/2}\right)+\nu\frac{1}{\Delta y^2}\left(v^*{}_{i,j+1}-2v^*{}_{i,j}-v^*{}_{i,j-1}\right)$$
$$-\frac{1}{\Delta y}\left(p^n{}_{i,j+1/2}-p^n{}_{i,j-1/2}\right)+f_y^{n+1/2} \tag{11}$$

The linearization below is used to obtain an efficient fractional-step method solution.

$$\hat{u}^2=u^{n2}+2u^n\left(\hat{u}-u^n\right)+0\left(\Delta t^2\right) \tag{12}$$

$$\hat{u}\hat{v}=u^n v^n+u^n\left(\hat{v}-v^n\right)+0\left(\Delta t^2\right) \tag{13}$$

$$u^*v^*=\hat{u}\hat{v}+\hat{v}\left(u^*-\hat{u}\right)+0\left(\Delta t^2\right) \tag{14}$$

$$v^{*2}=\hat{v}^2+2\hat{v}\left(v^*-\hat{v}\right)+0\left(\Delta t^2\right) \tag{15}$$

Next, substitute these equations into equations (8) – (11) to obtain the instantaneous velocity value $\hat{u}, \hat{v}, u^*, v^*$. In the first step, the instantaneous velocity value is obtained $\hat{u}, \hat{v}$ using the FDM finite difference method as follows,

$$\hat{u}_{i,j} + \Delta t.L_x\left(2u^n.\hat{u}\right)_{i,j} - \nu.\Delta t.L_{xx}\left(\hat{u}_{i,j}\right) = u^n_{i,j} + \Delta t.L_x\left(u^2\right)^n_{i,j} \tag{16}$$

$$\hat{v}_{i,j} + \Delta t.L_x\left(u^n.\hat{v}\right)_{i,j} - \nu.\Delta t.L_{xx}\left(\hat{v}_{i,j}\right) = v^n_{i,j} \tag{17}$$

Next, for the second half-step, the transient velocity value is obtained from the finite difference approach u^*, v^* as follows,

$$u^*_{i,j} + \Delta t.L_y\left(\hat{v}u^*\right)_{i,j} - \nu.\Delta t.L_{yy}\left(u^*_{i,j}\right) = \hat{u}_{i,j} + \Delta t.g_x \tag{18}$$

$$v^*_{i,j} + \Delta t.Ly\left(2\hat{v}u^*\right)_{i,j} - \nu.\Delta t.L_{yy}\left(\hat{v}^*_{i,j}\right) = \hat{v}_{i,j} + \Delta t.Ly\left(\hat{v}^2_{i,j}\right) + \Delta t.g_x \tag{19}$$

The transient and transient velocity equations above form a tridiagonal system which is solved by the Thomas method TDMA algorithm. The boundary values of the velocities $\hat{u}, \hat{v}, u^*, v^*$ are inserted into the tridiagonal system equations (see Roache 1976, Peyret and Taylor 2012, Lemos 1994) for a more detailed description [18]–[20].

2.2.2. Pressure Correction Equation [9]

$$\frac{1}{\Delta x^2}\left(\frac{p_{i+1,j} - p_{i,j}}{p^n_{i+1,j} + p^n_{i,j}} - \frac{p_{i,j} - p_{i-1,j}}{p^n_{i,j} + p^n_{i-1,j}}\right) + \frac{1}{\Delta y^2}\left(\frac{p_{i,j+1} - p_{i,j}}{p^n_{i,j+1} + p^n_{i,j}} - \frac{p_{i,j} - p_{i,j-1}}{p^n_{i,j} + p^n_{i,j-1}}\right) = \frac{1}{2\Delta t}\left(\frac{u^*_{i+\frac{1}{2},j} + u^*_{i-\frac{1}{2},j}}{\Delta x} + \frac{v^*_{i,j+\frac{1}{2}} + v^*_{i,j-\frac{1}{2}}}{\Delta y}\right) \tag{20}$$

2.2.3. Front-Tracking Method and Surface Tension

Front-Tracking method is a method used in tracking different fluid interfaces. There are 2 steps in the front tracking method, namely the first is moving the interface and constructing the density field. Generally, the interface is structured by adding and deleting points when the interface begins to form. For 2-D flow, it is relatively easier to create the data structure. Here is the use of a simple arrangement of points where there is an interface by marking its coordinates.

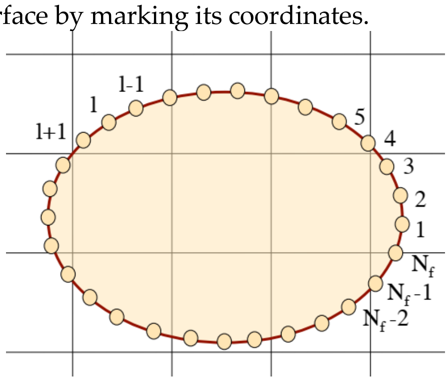

Figure 3. Marker points used to mark the interface between two fluids

Surface tension is one of the factors that determine the results of the modeling. Surface tension works only at the interface of two different fluids. To enable us to build the force per unit volume on a fixed grid, we must determine the total force acting on the interface portion using the following equation,

$$\delta f_{\sigma}^{l} = \sigma \int_{\Delta sl} \frac{\partial t}{\partial s} ds = \sigma\left(t_{l+1/2} - t_{l-1/2}\right) \tag{21}$$

Where surface tension is denoted by f , σ is the coefficient of surface tension and *t* is the tangent to the surface.

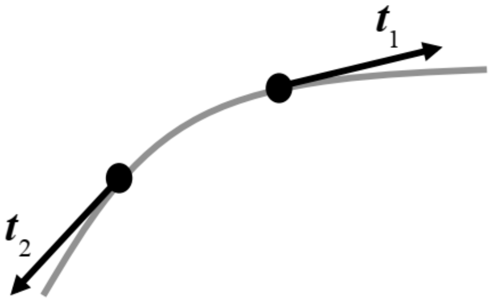

Figure 4. Surface tension at a confined interface segment.

2.2.4. Numeric Code (MATLAB)

Discretization of the governing equations described above is interpreted into code or script using MATLAB R2024a program with license number 41245703. With variations in density values, this script is run to simulate the motion of droplets when falling and hitting the surface. The script used is a development and modification of an existing script, where Tryggvason 2012 [9] uses an explicit scheme to solve the momentum equation while this study uses an implicit scheme.

3. Results

The phenomenon of a single droplet falling freely until it hits a solid surface is modeled in this study using Finite Volume Method with algorithmic equation solving or using an implicit scheme. This study is a continuation of what researchers have done in 2018 and 2024 [12], [13]. The focus of this study is studying how the density ratio affects the spreading factor, apex height, spreading velocity and pressure distribution in the droplet. This modeling has been validated with the modeling developed by Tryggvason 2012 [9]which uses an explicit scheme in solving the governing equation algorithm. Referring to the article, it is obtained that the modeling developed by these two studies is in accordance with each other.

Table 1. shows in detail the variation of single droplet phenomena in this study. The variation of the density ratio ($\rho^* = \rho_d / \rho_s$) was carried out to obtain more in-depth results regarding how variations in density affect the properties of droplet movements striking a surface.

Table 1. Variations of single droplet modeling.

Cases	Grid Size	Density Ratio (ρ_d / ρ_s)	Change in Time (Δt) s
1	164 x 164	20	125×10^{-5}
2	164 x 164	30	125×10^{-6}
3	164 x 164	50	125×10^{-6}
4	164 x 164	70	125×10^{-6}
5	164 x 164	80	125×10^{-7}
6	164 x 164	100	125×10^{-7}

3.1. Spreading Factor

The non-dimensional diameter is represented by the spreading diameter *at* a certain time divided by the initial diameter (D/d_o). The dimensionless time is represented by $t^* = (tv_o/d_d)$. The droplet diameter fluctuates and becomes stable after $t* = 1.3$. In general, the pattern of droplet diameter changes when hitting the surface for each case has the same tendency. The largest spreading diameter is achieved sequentially from $\varrho^* = 100$ to $\varrho^* = 20$ at t = 0.618 s. The Spreading Factor value for each case is shown in the following figure 5. and table 2.

Table 2. Spreading diameter in mm units for each variation of density ratio.

Time (s)	$\varrho^* = 20$	$\varrho^* = 30$	$\varrho^* = 50$	$\varrho^* = 70$	$\varrho^* = 80$	$\varrho^* = 100$
0.01	0.0021	0.0021	0.0021	0.0021	0.0021	0.0021
0.453	0.0024	0.0061	0.0061	0.0064	0.0067	0.0079
0.618	0.0062	0.0065	0.0065	0.0073	0.0091	0.0098
1.03	0.0026	0.0029	0.0029	0.0061	0.0065	0.0069
2.02	0.0022	0.0024	0.0024	0.0025	0.0025	0.0028

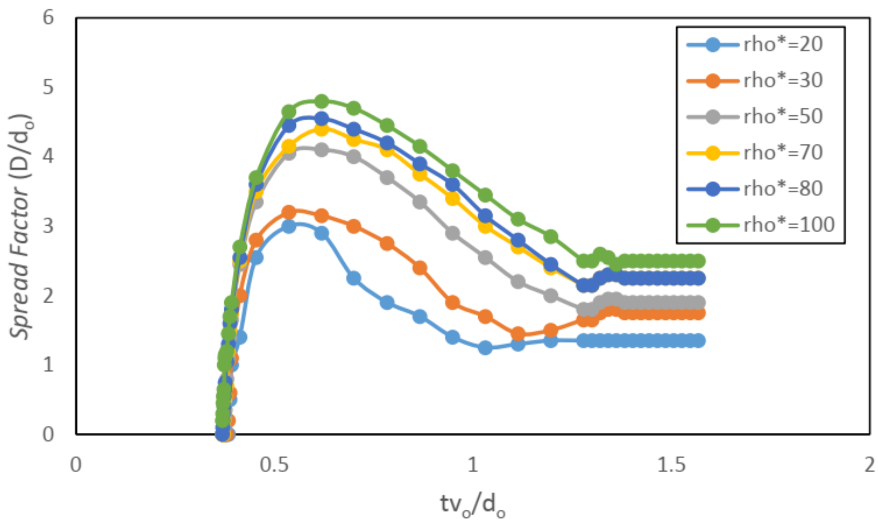

Figure 5. Non dimensional diameter spreading factor in relation to (tv_o/d_d)

3.2. Apex Height

The ratio of the droplet height value at a certain t to the initial droplet diameter is defined as the Apex Height. Non-dimensional time is represented by $t^* = (tv_o/d_d)$. Figure 6. and Table 3 show a significant decrease in droplet height when the droplet hits a solid surface caused by the impact velocity *and* until the droplet reaches a minimum height. The increasing value of the density ratio decreases the minimum droplet height. The minimum droplet height in the apex value for cases with density ratios of 30, 80 and 100 are respectively 0.26, 0.21 and 0.18.

3.3. Spreading Velocity

The spreading velocity is obtained from the calculation of the change in the droplet spreading diameter (ΔD_s) divided by the change in time from the initial position to a certain position (Δt). The spreading velocity of the droplet when it hits the surface is shown in Figure 6. The pattern of changes in spreading velocity has the same tendency for each case. The maximum spreading velocity occurs when $t^* = 0.453$ for each variation of the density ratio ϱ^*. From Figure 7, it is known that the greater the density ratio, the higher the spreading velocity *value*.

Table 3. Non-dimensional Apex Height conditions $\varrho^* = 30$, 80 and 100.

Time (s)	ϱ^* =30	ϱ^* =80	ϱ^* =100
0.01	0.95	0.95	0.95
0.453	0.35	0.31	0.27
0.618	0.26	0.21	0.18
1.03	0.65	0.55	0.55
2.02	0.55	0.47	0.43
0.01	0.95	0.95	0.95

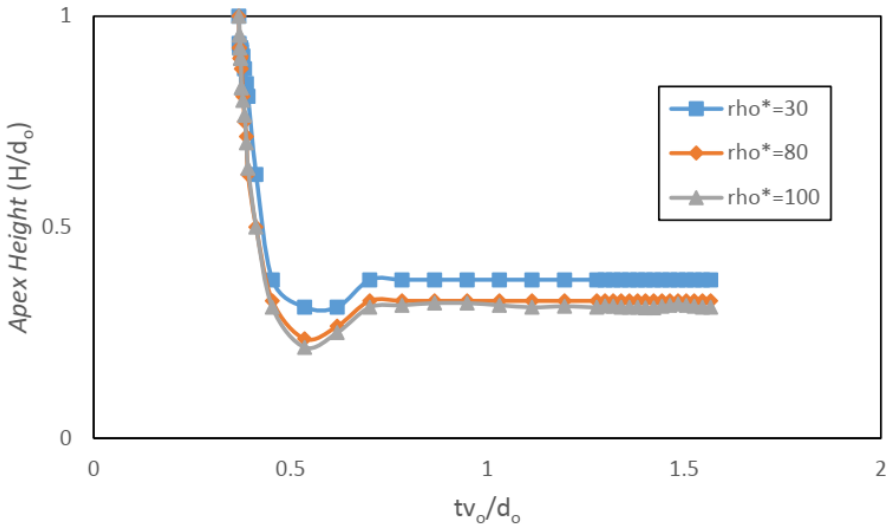

Figure 6. Non-dimensional diameter apex height in relation to (tv_o / d_d)

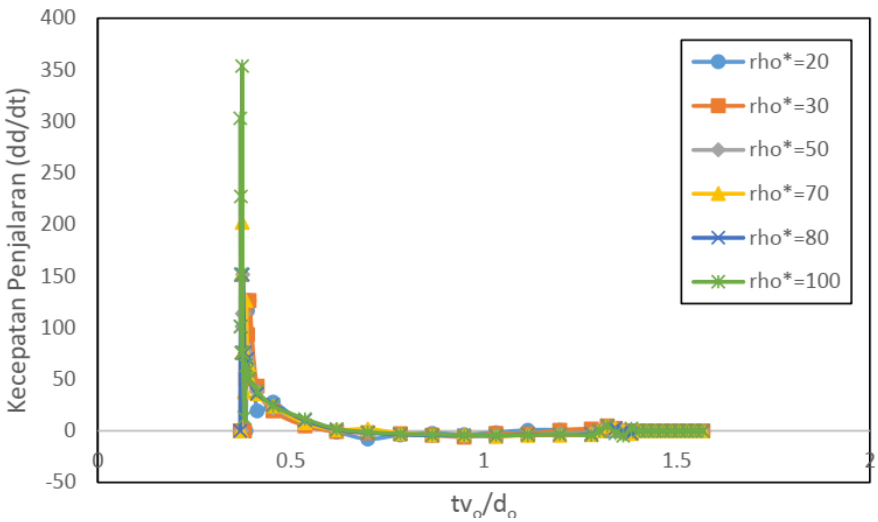

Figure 7. Non-dimensional diameter spreading velocity as a function of (tv_o / d_d)

3.4. Distribution of Pressure Inside Droplet when Hitting a Surface

Table 4 shows the pattern of pressure changes inside the droplet when it hits the surface over time for the density ratio $\varrho^* = 100$. The function of time is represented by the non-dimensional value $t^* = (tv_o/d_d)$ and the pressure is represented by the non-dimensional value $p^* = (p/\varrho.g.d_d)$. The droplet hits the surface at time $t* = 0.37$. At this condition, there is a significant pressure change due to the collision. A region with high pressure is seen around the collision point between the droplet and the solid surface [21]. The pressure spreads radially along the surface, moving towards and away from the edge until the pressure decreases until the droplet experiences a stable condition.

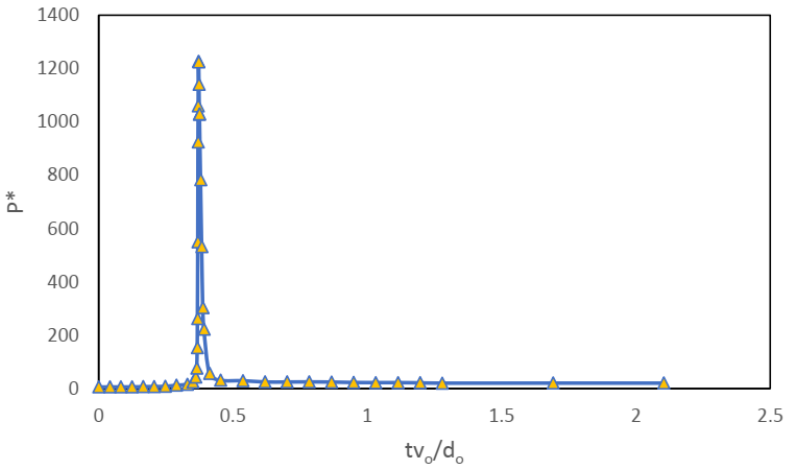

Figure 8. Pressure change as a function of time for a density ratio of 100.

As can be seen from Figure 8, the pressure at t ∗ = 0 − 0.4 first increases as the droplet moves downward. At t ∗ = 0.4 − 0.5, there is a significant increase in pressure. This indicates that the droplet experiences a spreading phenomenon. Then the pressure decreases until the droplet experiences a stable condition after t ∗ = 0.5.

3.5. Comparison to Previous Research

Figure 9. shows a comparison of the spread factor data in this study with those of Wu et al. (2015) and Endang et al. (2020). When hitting the surface, the droplet diameter gradually declines until it reaches a steady state after increasing noticeably to its maximume value. Overall, the droplet movement pattern in the dimensionless spreading factor value is in accordance with the results of the studies of Wu et al. (2015) and Endang et al. (2020). There is a difference in the time of the maximum spread factor because the density ratio between the droplet and the surrounding fluid is different for each study.

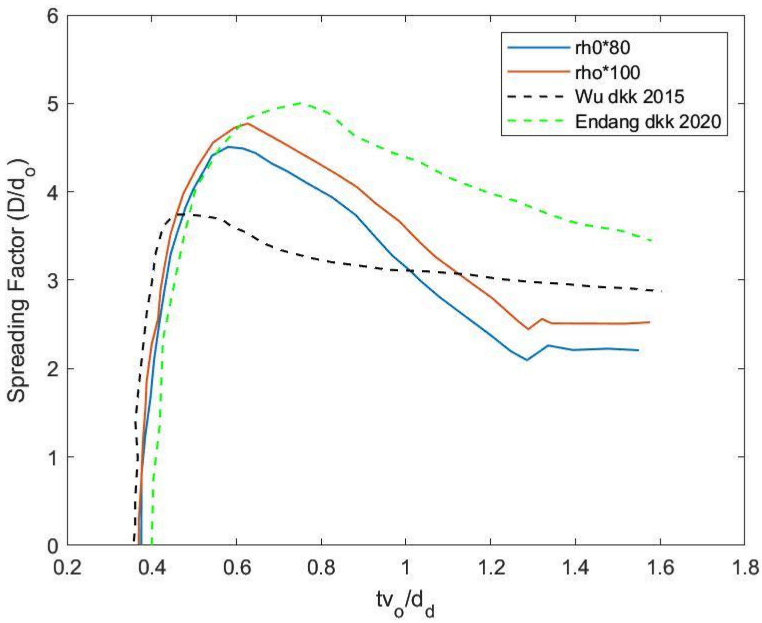

Figure 9. Comparison of the Spread Factor of this study (ϱ* = 80, ϱ* = 100) with data from Wu et al. (2015) [14]and Endang et al. (2020) [11].

 doi: 10.47355/AVIA.V6I2.137

Table 4. Non-dimensional Apex Height conditions ϱ * = 30, 80 and 100

tv_o/d_o	Distribusi tekanan	P* = P/(ϱ.g.do)
0,16		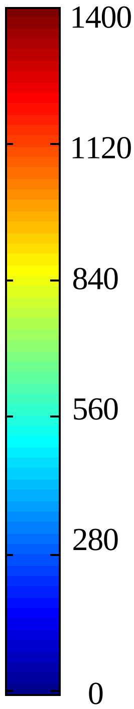
0,2		
0,28	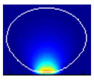	
0,37	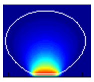	
0,374	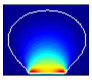	
0,375	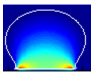	
0,379	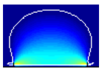	
0,383		
0,387		
0,391		
0,412		
0,618		
0,78		
0,948		
1,278		

4. Conclusions

This study is a development of previous droplet phenomenon modeling using the Finite Volume Method - Front Tracking with an implicit scheme. The focus of this study is to determine the effect of surface tension involvement and variations in the density ratio on the measured variables, namely spreading factor, apex height, spreading velocity and pressure distribution in the droplet. Modeling with this method can track the droplet interface and the surrounding fluid well with a density ratio reaching ϱ * = 100. The density ratio greatly affects the measured variables. The greater the value of the density ratio, the maximum diameter of the droplet during Spreading increases in line with the spreading factor and spreading velocity values. Conversely, the greater the value of the density ratio, the lower the apex height value.

Acknowledgments
The Department of Mechanical, Faculty of Engineering, University of Lampung, is greatly appreciated by the authors for facilitating this study.

References

1. D. Taglienti, F. Guglietta, and M. Sbragaglia, "Droplet dynamics in homogeneous isotropic turbulence with the immersed boundary-lattice Boltzmann method.," *Phys. Rev. E*, vol. 110 1–2, p. 15302, 2024, doi: 10.1103/physreve.110.015302.
2. S. Belgaonkar, B. Bamble, A. Barve, and B. Kumar, "Visualization of Droplet Dynamics in Cloud," *ITM Web Conf.*, 2020, doi: 10.1051/itmconf/20203203033.
3. L. Jin and Y. Wang, "Numerical study on surface-heterogeneity-induced anisotropic impact dynamics of droplet," *Colloid Interface Sci. Commun.*, vol. 44, p. 100495, 2021.
4. T. T. Nguyen, D. B. Luu, N. H. Tran, and M. S. Tran, "Study on the velocity of droplet at steady state in contraction microchannels by numerical simulation," *Vietnam J. Mech.*, vol. 45, no. 4, pp. 287–295, 2023.
5. A. Langins, A. P. Stikuts, and A. Cēbers, "A 3D BEM algorithm for simulations of magnetic fluid droplet dynamics," *arXiv Prepr. arXiv2203.09499*, 2022.
6. K. El Kadi, M. I. H. Ali, M. D. D. Islam, and I. Janajreh, "Understanding Saline Water Droplet-Membrane Surface Interaction Using Molecular Dynamics Simulations," in *Heat Transfer Summer Conference*, American Society of Mechanical Engineers, 2023, p. V001T13A003.
7. M. Muradoglu and A. D. Kayaalp, "An auxiliary grid method for computations of multiphase flows in complex geometries," *J. Comput. Phys.*, vol. 214, no. 2, pp. 858–877, 2006.
8. M. Muradoglu and S. Tasoglu, "A front-tracking method for computational modeling of impact and spreading of viscous droplets on solid walls," *Comput. Fluids*, vol. 39, no. 4, pp. 615–625, 2010.
9. G. Tryggvason, "A Front-tracking/Finite-Volume Navier-Stokes Solver for Direct Numerical Simulations of Multiphase Flows," 2012.
10. K. Nandakumar Chandran, P. T. Naveen, R. Abhilash, and S. Kumar Ranjith, "Theoretical modelling of droplet extension on hydrophobic surfaces," *Int. J. Comut. Fluid Dyn.*, vol. 35, no. 7, pp. 534–548, 2021.
11. E. Mawarsih, E. P. Budiana, Deendarlianto, Indarto, and S. Kamal, "Numerical simulation of single droplet phenomenon using method finite difference and front-tracking," *AIP Conf. Proc.*, vol. 2296, no. January 2019, 2020, doi: 10.1063/5.0030454.
12. D. Kurniawan and A. D. Prabowo, "Numerical Simulation of Single Droplet Phenomenon to Investigate Density Field Characteristics Using Finite Volume-Front Tracking Method," *J. Appl. Sci. Eng. Technol.*, vol. 4, no. 2, pp. 35–45, 2024.
13. D. Kurniawan, E. Budiana, D. Deendarlianto, and I. Indarto, "Simulasi Numerik Fenomena Single Droplet Menggunakan Metode Volume Hingga dan Front-Tracking," *POROS*, vol. 15, no. 2, pp. 84–91, 2017.
14. J. Wu, J. J. Huang, and W. W. Yan, "Lattice Boltzmann investigation of droplets impact behaviors onto a solid substrate," *Colloids Surfaces A Physicochem. Eng. Asp.*, vol. 484, pp. 318–328, 2015.
15. M. F. Tomé, J. L. Doricio, A. Castelo, J. A. Cuminato, and S. McKee, "Solving viscoelastic free surface flows of a second-order fluid using a marker-and-cell approach," *Int. J. Numer. methods fluids*, vol. 53, no. 4, pp. 599–627, 2007.
16. D. P. Trebotich and P. Colella, "A Projection Method for Incompressible Viscous Flow on Moving QuadrilateralGrids," *J. Comput. Phys.*, vol. 166, no. 2, pp. 191–217, 2001, doi: https://doi.org/10.1006/jcph.2000.6654.
17. D. Drikakis and W. Rider, Eds., "Projection Methods: The Basic Theory and the Exact Projection Method BT - High-Resolution Methods for Incompressible and Low-Speed Flows," Berlin, Heidelberg: Springer Berlin Heidelberg, 2005, pp. 209–235. doi: 10.1007/3-540-26454-X_11.
18. P. J. Roache, "Computational fluid dynamics," *Comput. Fluid Dyn.*, 1976.
19. R. Peyret and T. D. Taylor, *Computational methods for fluid flow*. Springer Science & Business Media, 2012.

20. C. M. Lemos, "FDFLOW: a FORTRAN-77 solver for 2-D incompressible fluid flow," *Comput. Geosci.*, vol. 20, no. 3, pp. 265–291, 1994.
21. Z. Zhao *et al.*, "Regulating droplet impact symmetry by surface engineering," *Droplet*, vol. 2, no. 2, p. e52, 2023.